OPEN ACCESS

KING'S College LONDON

King's Research Portal

DOI:
10.1002/stem.2263

Document Version
Peer reviewed version

Link to publication record in King's Research Portal

Citation for published version (APA):
Marteyn, A., Sarrazin, N., Yan, J., Bachelin, C., Deboux, C., Santin, M. D., Gressens, P., Zujovic, V., & Baron-Van Evercooren, A. (2016). Modulation of the Innate Immune Response by Human Neural Precursors Prevails over Oligodendrocyte Progenitor Remyelination to Rescue a Severe Model of Pelizaeus-Merzbacher Disease. *Stem Cells*, *34*(4), 984-96. https://doi.org/10.1002/stem.2263

Citing this paper
Please note that where the full-text provided on King's Research Portal is the Author Accepted Manuscript or Post-Print version this may differ from the final Published version. If citing, it is advised that you check and use the publisher's definitive version for pagination, volume/issue, and date of publication details. And where the final published version is provided on the Research Portal, if citing you are again advised to check the publisher's website for any subsequent corrections.

General rights
Copyright and moral rights for the publications made accessible in the Research Portal are retained by the authors and/or other copyright owners and it is a condition of accessing publications that users recognize and abide by the legal requirements associated with these rights.

•Users may download and print one copy of any publication from the Research Portal for the purpose of private study or research.
•You may not further distribute the material or use it for any profit-making activity or commercial gain
•You may freely distribute the URL identifying the publication in the Research Portal

Take down policy
If you believe that this document breaches copyright please contact librarypure@kcl.ac.uk providing details, and we will remove access to the work immediately and investigate your claim.

Download date: 05. May. 2023

Running head: Immunomodulation is required to rescue PMD

Modulation of the innate immune response by human neural precursors prevails over oligodendrocyte progenitor remyelination to rescue a severe model of Pelizaeus-Merzbacher disease

Authors: Antoine Marteyn[1,2,3], Nadège Sarrazin[1,2,3], Jun Yan[5,6], Corinne Bachelin[1,2,3], Cyrille Deboux[1,2,3], Mathieu D. Santin[1,2,3,4], Pierre Gressens[5,6], Violetta Zujovic[1,2,3], Anne Baron-Van Evercooren[1,2,3]

Institutions:

[1]INSERM, U1127, Institut du Cerveau et de la Moelle épinière, 75651 Paris cedex 13, France.

[2]Université Pierre et Marie Curie-Paris 6, UMR_S 1127, Paris, France.

[3]CNRS, UMR 7225, Paris, France.

[4]CENIR, Centre de NeuroImagerie de Recherche, ICM, Hôpital Pitié-Salpêtrière, Paris, France.

[5]INSERM, U1141, F-75019 Paris, France.

[6]Univerité Paris Diderot, Sorbonne Paris Cité, UMRS 1141, F-75019 Paris, France.

Author contributions:

Antoine Marteyn: conception and design, collection and assembly of data, data analysis and interpretation, manuscript writing;

Nadège Sarrazin: conception and design, collection and assembly of data, data analysis and interpretation;

ScholarOne Support: (434) 964-4100

For Peer Review

Jun Yan: collection and assembly of data, data analysis and interpretation;

Corinne Bachelin: collection and assembly of data, data analysis and interpretation;

Cyrille Deboux: collection and assembly of data;

Mathieu Santin: collection and assembly of data;

Pierre Gressens: conception and design, data analysis and interpretation;

Violetta Zujovic: conception and design, collection and assembly of data, data analysis and interpretation, manuscript writing;

Anne Baron-Van Evercooren: conception and design, financial support, administrative support, data analysis and interpretation, manuscript writing, final approval of manuscript.

Correspondence to: Anne Baron-Van Evercooren, PhD

INSERM U1127, Institut du Cerveau et de la Moelle épinière (ICM),

47 Bd de l'Hôpital, 75013, Paris, France

Phone: +33 1 57 27 41 23

E-mail: anne.baron@upmc.fr

Keywords: Pelizaeus-Merzbacher disease (PMD); cell-based therapy; human neural precursor cells (hNPCs); remyelination; modulation of inflammation.

For Peer Review

Abstract

Pelizaeus-Merzbacher disease (PMD) results from an X-linked misexpression of proteolipid protein 1 (PLP1). This leukodystrophy causes severe hypomyelination with progressive inflammation, leading to neurological dysfunctions and shortened life expectancy. While no cure exist for PMD, experimental cell-based therapy in the dysmyelinated *shiverer* model suggested that human oligodendrocyte progenitor cells (hOPCs) or human neural precursor cells (hNPCs) are promising candidates to treat myelinopathies. However, the fate and restorative advantages of human NPCs/OPCs in a relevant model of PMD has not yet been addressed. Using a model of *Plp1* overexpression, resulting in demyelination with progressive inflammation, we compared side-by-side the therapeutic benefits of intracerebrally grafted hNPCs and hOPCs. Our findings reveal equal integration of the donor cells within presumptive white matter tracks. While the onset of exogenous remyelination was earlier in hOPCs-grafted mice than in hNPC-grafted mice, extended lifespan occurred only in hNPCs-grafted animals. This improved survival was correlated with reduced neuroinflammation (microglial and astrocytosis loads) and microglia polarization towards M2-like phenotype followed by remyelination. Thus modulation of neuroinflammation combined with myelin restoration is crucial to prevent PMD pathology progression and ensure successful rescue of PMD mice. These findings should help to design novel therapeutic strategies combining immunomodulation and stem/progenitor cell-based therapy for disorders associating hypomyelination with inflammation as observed in PMD.

Introduction

Pelizaeus-Merzbacher disease (PMD) results from proteolipid protein 1 (PLP1) gene mutations. It is a rare hypomyelinating leukodystrophy characterized by delayed motor and cognitive development, nystagmus, ataxia, hypotonia, and spasticity in the first year of life. The severity and onset of this X-linked recessive degenerative central nervous system (CNS)

ScholarOne Support: (434) 964-4100

For Peer Review

disorder depends upon the nature of *PLP1* mutations, which include duplication and point mutations. Changes in expression of myelin proteins are associated with progressive hypertrophic astrogliosis and massive microglial activation in animal models of PMD [1-3] and in man [4, 5]. Interestingly, microglia/macrophage activation varies with disease severity in PMD patients and *PLP1* mutant mice, indicating that the inflammatory response to *PLP1* gene mutations is conserved among species [5]. Complete *PLP1* gene duplication (62%) [6] is the most common cause of PMD and leads to marked CNS hypomyelination. This mutation increases *PLP1* gene dosage [7] primarily causing toxic PLP1 accumulation in oligodendrocyte endoplasmic reticulum [8], leading to microglial activation and oligodendrocyte death [9]. As *PLP1* is fully conserved between mouse and human and no spontaneous duplication of *Plp1* exists in animal models, several transgenic mice overexpressing *Plp1* were generated to decipher PMD pathohysiology [7, 10]. The transgenic *Plp-tg* line #66, exhibiting a 2-fold transcriptional overexpression of *Plp1*, is the most relevant model of PMD with *Plp1* duplication [11]. Mice phenotype includes severe hypomyelination, progressive astrocytosis and microglial activation, seizures, motor and sensory deficits and a shortened lifespan [7], as in PMD patients [5, 12].

While there is currently no cure for PMD, transplantation of neural precursor cells (NPCs) or oligodendrocyte progenitor cells (OPCs) has emerged as a promising approach to replace affected oligodendrocytes. Indeed, successful myelination was achieved after engraftment of human NPCs [13, 14] and OPCs [15, 16] derived from fetal brain or differentiated from induced pluripotent stem cells (iPS) [17] in the immunodeficient dysmyelinated *shiverer* model. Extended lifespan of *shiverer* mice has been reported after transplantation with hOPCs [18] but not with hNPCs, suggesting that hOPCs might be the best cell candidate to treat myelin disorders such as PMD [15, 19, 20]. On the other hand, NPCs could have an advantage compared to OPCs in diseases associating demyelination and inflammation like

For Peer Review

ScholarOne Support: (434) 964-4100

PMD. Indeed, NPCs that release multiple neurotrophins and cytokines, have been shown to attenuate brain inflammation after delivery in inflammatory models of multiple sclerosis [21-24], and to decrease classically activated (M1-like) macrophages in severely contused spinal cord [25]. Although *shiverer* mice, due to their MBP deficiency, are an excellent model system to trace donor-derived myelin, these mice are not representative of PMD since they do not display mutations in the *Plp1* gene, nor do they reflect the noxious inflammatory component of PMD [3, 5, 26]. To date the therapeutic benefits of hNPCs and/or hOPCs after transplantation in a relevant model of PMD, such as *Plp1* duplication, characterized by demyelination and progressive inflammation, is still lacking. Understanding the therapeutic impact of each cell type when facing such noxious environment would foster successful translation of stem cell-based therapy from bench to clinic.

In this study, we took advantage of the *Plp-tg* line #66 that faithfully mimics PMD duplication. We crossed *Plp-tg* mice over the *Rag null* background (*Plp-tg:Rag*) to prevent rejection of the human donor cells and compared in parallel the therapeutic benefits of intracerebrally grafted hNPCs and hOPCs. We report that upon transplantation in the neonate immunodeficient *Plp1* overexpressing mice, both cell types integrated equally well in the PMD environment. While each cell type functionally replaced the host deficient oligodendrocytes within the time-frame corresponding to their differentiation stage, only hNPCs rescued the severely affected PMD mice. The impressive therapeutic benefit of hNPCs was directly correlated with their ability to modulate inflammation prior to remyelination. These data indicate that inflammatory modulation is a pre-requisite to myelin restoration to promote survival and clinical recovery of PMD mice. They also suggest promising perspectives of combining immunomodulation and stem/progenitor cell-based therapy for myelin disorders associating hypomyelination with inflammation.

For Peer Review

ScholarOne Support: (434) 964-4100

Materials and Methods

Mouse line

Plp-tg mice (mouse line #66), overexpressing *Plp1* genes resulted from the autosomal insertion of a transgene comprising seven copies of the wild type murine *Plp1* gene [7]. To avoid cell rejection, homozygous *Plp-tg* mice were crossed to homozygous *recombination activating gene-2* null immunodeficient mice to generate *Plp-tg:Rag* mice (tg66/tg66 x $Rag2^{-/-}$). *Shiverer:*$Rag2^{-/-}$ mice were used in this study to confirm the timing of myelination by the different transplanted cells. These mice were generously provided by S. Goldman's laboratory [16].

hNPCs culture

Human foetuses were obtained after legal abortion according to the recommendations of the Agence de la Biomedecine (agreement #003187) with the written consent of the patients. hNPCs were isolated from lateral ganglionic eminences of human foetuses (7 to 9 weeks of gestation) as previously described [13]. They were amplified in spheres in N medium (consisting of a 1:1 mixture of Dulbecco's modified Eagle's medium-F12 supplemented with 1% N2 supplement; 0.5% B27; 5 mM HEPES (all Life technologies); 20 ng/ml insulin (Eurogenetec); 6 mg/ml glucose (Sigma) supplemented with 20 ng/ml basic fibroblast growth factor and 20 ng/ml epidermal growth factor (Peprotech).

CMV-GFP transduction of hNPCs

For their traceability after transplantation, hNPCs were transduced with the cytomegalovirus-green fluorescent protein (CMV-GFP) lentiviral vector at an MOI of 1.1. Efficiency of

ScholarOne Support: (434) 964-4100

For Peer Review

transduction (>90%) was determined on fixed cells by immunocytochemistry using a chicken anti-GFP antibody at (1:500, Aves, GFP-1020).

hOPCs production and CD140a/PDGFRα cell sorting

To generate hOPCs, hNPCs were induced to differentiate after seeding onto polyornithine/laminin-coated dishes, and feeding during 3 weeks with N medium, supplemented with PDGF-AA (10 ng/ml) (Sigma-Aldrich), bFGF and EGF (20 ng/ml). Medium was changed every 2-3 days. Flow cytometry of hOPCs-derived hNPCs was performed with a FACSAria III (Becton Dickinson) after cell dissociation using Accumax (Sigma) and 30 minutes incubation on ice with the following antibodies: mouse anti-human CD140a-PE-conjugated antibodies (1:50, BD, 556001), and mouse anti-human IgG2a-PE-conjugated (1:50, BD, 554648). This procedure allowed the selection of 17.2 ± 1.2% of CD140a/PDGFRα^{+} cells in 6 independent experiments. After sorting, cells were washed and either processed for RNA extraction, plated for immunocytochemical characterization or directly resuspended at 10^5 cells per µl into DMEM medium for transplantation.

Isolation of CD11+ cell from corpus callosum of *Plp-tg:Rag* mice

Fifteen week old *Plp-tg:Rag* mice (n=4) of each group (hNPCs-grafted, hOPCs-grafted and ungrafted) were anesthetized with pentobarbital (50mg/kg) and then sacrificed by transcardiac perfusion with PBS 1X. Corpora callosa were isolated and dissociated using the "neural tissue dissociation kit (P)" (Miltenyi) in combination with the gentleMACS Dissociator. In order to significantly improve CD11b staining of the resulting single-cell suspensions, myelin debris were removed according to "myelin removal beads II" instructions (Myltenyi). Finally, CD11b+ cells were magnetically labeled with "CD11b MicroBeads" (Miltenyi) and harvested on the MACS Separator.

ScholarOne Support: (434) 964-4100

For Peer Review

RNA Extraction and Real-Time RT-PCR

Total RNA from unsorted cells and CD140a resulting fractions were extracted according to the RNeasy Mini Protocol (Qiagen). Reverse transcription was performed with SuperScript III reverse transcriptase (Life technologies). Real-time PCR was performed with Light Cycler 480 SYBR Green I Master (Roche) using the LightCycler® 480 System. The following primers were used for RT-PCR: *Cyclophilin A* forward (Fw) 5'-CCCACCGTGTTCTTCGACAT-3', *Cyclophilin A* reverse (Rev) 5'-CCAGTGCTCAGAGCACGAAA-3', *PDGFRalpha* Fw 5'-TTGACAACCTCTACACCACACTGA-3', *PDGFRalpha* Rev 5'-TCCGGTACCCACTCTTGATCTTAT ; *TuJI* Fw 5'- GGCCTGACAATTTCATCTTTGG -3', *TuJI* Rev 5'-ACCACATCCAGGACCGAATC-3', *MAP5* Fw 5'-CTGTGGAAAAGGCAGCAAAAC -3', *MAP5* Rev 5'-CAGCATTCTTGGTCTCCTTGTCT-3'.

Primers used to quantify M1-like and M2-like gene expression of $CD11b^+$ cells, isolated from the corpora callosa of hNPCs / hOPCs-grafted and ungrafted (homozygous) *Plp-tg:Rag* mice, were designed according to Chhor et al., 2013 [27].

Primary microglial culture

Primary mixed glial cell cultures were prepared from newborn C57BL/6 mouse brain. After removal of the meninges, cortices were dissociated and the resulting cell suspension was resuspended in Dulbecco's modified Eagle's medium supplemented with 10% foetal bovine serum (all Life Technologies). Microglial cells were isolated from this primary mixed glial culture on day 14 by shaking before plating at 20,000 cells / cm^2. The following day, microglial cells were treated for 24h with IFNγ at 100 µg/mL or IL-4 at 50 µg/mL (R&D

ScholarOne Support: (434) 964-4100

For Peer Review

Systems) to polarize microglia to a M1-like or a M2-like phenotype respectively. Cells were then lysed, RNAs extracted, and used as positive control for *in vivo* $CD11b^+$ cell gene expression analysis.

Transplantation

At postnatal day 1, newborn pups were cryoanesthetized before bilateral injections (10^5 cells/1 µl) rostral to the corpus callosum, 1 mm caudally, 1 mm laterally from bregma and at a depth of 1 mm.

Immunohistochemistry

For immunohistochemistry, mice were sacrificed by transcardiac perfusion-fixation with 4% paraformaldehyde. Brains were sectioned horizontally at 12 µm thickness with a cryostat (CM3050S; Leica). *In vivo* characterization of grafted cells was performed by immunostaining using the following antibodies: anti-human NOGO-A (1:100, Santa Cruz Biotechnology, sc-11030), anti-PDGFR alpha (1:100, Santa Cruz Biotechnology, sc-338)), anti-APC (CC1, 1:100, Calbiochem, OP80), anti-MBP (1:400, Chemicon, AB980), anti-Olig2 (1:500, Chemicon, AB9610). Neuroinflammation was characterized by Iba1 (1:500, Wako, 019-19741) and GFAP (1:500, Dako, Z0334) staining, nodes of Ranvier, by Caspr (1:1000, generous gift from E. Peles, Rehovot, Israel) and Neurofascin (1:350, Abcam) staining, neuronal lineage by TuJI (1:100, Sigma, T8660) staining and proliferation by Ki67 (1:100, Dako, m7240) staining. For MBP, NOGO-A and Iba1 staining, sections were pre-treated with ethanol. Secondary antibodies conjugated with FITC, TRITC (SouthernBiotech) or Alexa Fluor 647 (Life Technologies) were used respectively at 1:100 and 1:1000. Nuclei were stained with Dapi (1 µg/ml, Sigma-Aldrich) (1:1,000). Imaging was performed with a fluorescent Apotome microscope (Zeiss) and Slide scanner (Nanozoomer, Hamamatsu).

For Peer Review

ScholarOne Support: (434) 964-4100

MRI

T2-weighted MRI images were acquired using 11.7 T MRI (BioSpec 117/16, Brüker) on ungrafted *Plp-tg:Rag* mice at 15 weeks. Mice were anesthetized using a mixture of isofluorane (5% for induction 1 1.5% for maintenance) gas and air at a flow rate of 1 L/min via a face mask. Mouse breathing rate was monitored throughout the experiment and body temperature was maintained at 38°C using circulating water.

Electron microscopy

For phenotype characterization, ungrafted *Plp-tg:Rag* mice were sacrificed at 4 weeks by transcardiac perfusion with 4% paraformaldehyde/2.5% glutaraldehyde (Euromedex). Brains were cut into 70 µm-thick pieces and fixed in 2% osmium tetroxide (Sigma) overnight.

For characterization of donor-derived myelin by immuno-electron microscopy, grafted animals were perfused with 4% paraformaldehyde and 0.025% glutaraldehyde (Electron Microscopy Science). Brains were removed and cut into 70 µm slices with a vibratome VT-1000S (Leica). For GFP immunodetection, slices were incubated overnight with anti-GFP (1:400, Nacalai Tesque, 04404-84) at 4°C, followed by 3 hours incubation at room temperature with biotin-conjugated anti-rat antibody (1:100, Jackson Beckman, 112-066-062), followed with streptavidin conjugated to beta-galactosidase (1:100, Vector, A-2300). Beta galactosidase was revealed by Bluo-Gal (Sigma) incubation for 3 hours at 37°C. Immunolabeled slices were then post-fixed with 2.5% glutaraldehyde for 2 h and 2% osmium tetroxide (Electron Microscopy Science) for 30 min. After dehydration, samples were embedded in epon. Ultra-thin sections were analyzed with a Hitachi HT7700 electron microscope.

For Peer Review

ScholarOne Support: (434) 964-4100

Behavioural assays

Global locomotor performances of grafted and ungrafted mice were evaluated using a rotarod (Letica, Barcelona, Spain) to measure coordination balance and motor control of hindlimbs. Tests were performed at 10, 15, 20 and 33 weeks post-grafting. Mice were placed on a rotating beam. The rod was set to accelerate from 4 to 40 revolutions per minute (rpm) over 30s and then maintained a constant speed.

Quantification analysis and statistical analysis

For in vivo analysis of differentiation and inflammation, 3-4 sections per animal and 3-5 animals per condition were analysed. Data collected with the Nanozoomer were analysed and quantified using the MorophoStrider software (Exploranova). The percentages of GFP^+ cells expressing APC or NOGO-A were established over the total number of GFP^+ cells. The extent of myelination or neuroinflammation corresponded to the MBP, GFAP or Iba1 labelled area divided by the whole corpus callosum area.

All statistical comparisons included Student's t test. The cut-off for statistical significance was set at $*p < 0.05$; $**p<0.01$; $***p<0.001$. Statistical analysis was performed with Statistica software. Data are shown as mean ± standard error of the mean (SEM).

Study approval

All animal care and experiments conformed to European Community regulations and INSERM ethical committee (authorization 75-348; 20/04/2005).

For Peer Review

ScholarOne Support: (434) 964-4100

Results

Characterization of Plp-tg:Rag mice

To prevent immune-rejection and facilitate analysis of transplanted human xenografts, *Plp*-overexpressing mice (line #66) were crossed with the immunodeficient strain *Rag2*$^{-/-}$. We first confirmed that the Rag2$^{-/-}$ phenotype did not alter the phenotype of the *Plp-tg* mice. Although myelination onsets after birth, widespread hypomyelination [7] was detected in all one month old homozygous *Plp-tg:Rag* brains as viewed by T2 weighted imaging (Fig. 1B) and confirmed by MBP immunolabeling (Fig. 1C, C'). Electron microscopy revealed very few myelinated axons (Fig. 1A). Immunohistochemistry for GFAP and Iba1 revealed astrogliosis (Fig. 1D, D') and activated microglial cells (Fig. 1E, E') confirming the strong inflammatory context in homozygous *Plp-tg:Rag*, even though T and B cells were absent. The preservation of these abnormalities was associated with seizures and premature death of the double transgenic mice around 20 weeks reflecting the original phenotype of the *Plp-tg* line.

Characterization of hNPCs and hOPCs

Human NPCs were isolated from lateral ganglionic eminences of three independent foetuses [13] and differentiated *in vitro* into hOPCs. We previously demonstrated after long-term *in vitro* amplification (100 days) that hNPCs conserved their immature state and their proliferative activity expressing, respectively, the neural stemness marker Nestin (98.5%) and proliferation marker Ki67 (42.6%), and only few differentiated cells expressing GFAP (5.6%), TuJ1 (2.1%), Olig2 (32.4%) and A2B5 (3.4%).. Moreover, these cells were multipotent after engraftment into the adult demyelinated nude spinal cord, and they successfully remyelinated the demyelinated adult *shiverer* spinal cord [13].

To avoid heterogeneity among cell sources, hOPCs were derived from the *in vitro* differentiation of these hNPCs, in the presence of platelet-derived growth factor (PDGF).

ScholarOne Support: (434) 964-4100

For Peer Review

After three weeks, cell cultures were specifically enriched in early hOPCs by fluorescence-activated cell sorting (FACS) using the OPC specific cell marker, CD140a/PDGFRα [15]. Consequently, CD140a positive cell fractions were all positive for CD140a/PDGFRα. The majority expressed Ki67 (>80%) and Olig2 (>90%). Moreover they showed a typical OPC bipolar phenotype (Fig. 2A-C). In contrast, the CD140a negative fractions did not express PDGFRα or Olig2 but displayed a neuronal phenotype and expressed the immature neuronal marker TuJ1 (>90%) (Fig. 2D-F). Both fractions were devoid of $GFAP^+$ cells (<0.01%). Quantitative RT-PCR confirmed enrichment of PDGFRα transcripts in the CD140a positive populations and of the neuronal Tuj1 and Map5 transcripts in the CD140a negative populations (Fig. 2G).

To better define the $CD140a^+/PDGFR\alpha^+$ sorted cells, we compared their myelinogenic potential to hNPCs after transplantation into newborn *shiverer:Rag* mice. In line with previous studies [15, 16], our results indicated faster myelinogenic capacity of hOPCs ($CD140a^+/PDGFR\alpha^+$) since they produced extensive myelin 15 weeks post transplantation (p.t.) while hNPCs produced myelin only at later times (Fig. 2H-I). Moreover, hOPCs transplants increased *shiverer:Rag* mice survival up to 30 weeks whereas hNPCs transplants extended survival only up to 25 weeks (Fig. 2J).

Grafted hNPCs improve Plp-tg:Rag mice lifespan and locomotion

We next evaluated the therapeutic outcome of hNPCs and hOPCs in the PMD model. We first assessed the effects of both cell types on survival and locomotion after bilateral cell injections (10^5 cells/µl) rostrally to the corpus callosum of postnatal day 1 *Plp-tg:Rag* mice. Surprisingly, while hOPCs grafts improved *shiverer:Rag* survival, they did not prolong lifespan of *Plp-tg:Rag* mice, which died prematurely at 19.6 ± 1.3 weeks. In contrast, hNPCs transplants significantly increased *Plp-tg:Rag* mice life expectancy (32,5 ± 2.9 weeks,

ScholarOne Support: (434) 964-4100

For Peer Review

p<0.001) compared to ungrafted mice (20.0 ± 0.6 weeks) (Fig. 3A-B). This value was strongly underestimated due to the multiple sacrifices performed to evaluate remyelination by MRI or electron microscopy after 25 weeks.

Hypomyelination in *Plp-tg:Rag* mice results in progressive hind limb weakness and consequently locomotor defects. We therefore evaluated motor coordination and balance by rotarod assay. Ungrafted *Plp-tg:Rag* mice showed increased balance deficits with age since rod fall latencies decreased from 14.7 ± 1.2 sec at 10 weeks p.t. to 10.9 ± 1.0 sec at 30 weeks p.t. Performances of hNPCs-grafted mice tended to be improved compared to ungrafted *Plp-tg:Rag* mice at every experimental time point (15.7 ± 1.0 sec at 10 weeks p.t. and 14.3 ± 1.5 sec at 30 weeks p.t.), and were significantly higher at 25 weeks p.t. (16.1 ± 0.9 sec vs 12.5 ± 0.9 sec).

Long-term cell survival and widespread migration is achieved equally by grafted hNPCs and hOPCs in Plp-tg:Rag mice

To decipher why hNPCs rescued *Plp-tg:Rag* mice in contrast to hOPCs, we first analysed survival and migratory potentials of the grafted cells. At 15 weeks p.t., both grafted cell types extensively invaded brain regions and more particularly the *fimbria* and the corpus callosum (Supplementary Data Fig. S1A). Evaluation of grafted cell density in the corpus callosum indicated that the percentage of integrated cells was similar for hNPCs (20.2 ± 3.3%) and hOPCs (27.4 ± 5.8%) (Supplementary Data Fig. S1B). Moreover, both grafted cell types were also found in other white matter structures such as cerebellum, striatum, anterior commissure or olfactory bulb, as illustrated for hNPCs (Supplementary Data Fig. S1C), highlighting their great capacity to migrate across the anterior-posterior and dorso-ventral axes from two rostral injection sites. Furthermore, both transplanted cell types had a great capacity to survive in the PMD environment since immunohistochemistry for Caspase 3 indicated low rates of cell

ScholarOne Support: (434) 964-4100

For Peer Review

death (<0.01%) at 15 weeks p.t. Excellent survival of the grafted cells was further confirmed by the detection of substantial populations of hNPCs in *Plp-tg:Rag* mice that survived up to 48 weeks p.t.

Grafted hNPCs and hOPCs mature into oligodendrocytes at different rates

We next assessed the capacity of grafted cells to differentiate into oligodendrocytes and generate functional myelin. At 15 weeks p.t., hOPCs had a mature morphology with multi-branched processes while hNPCs remained essentially as immature bipolar cells (Fig. 4A). Most hOPCs expressed APC (76.5 ± 5.5%) and human NOGO-A (38.7 ± 10.5%), whereas only a few hNPCs expressed these markers (respectively 15.8 ± 4.7% and 2.1 ± 0.9%) (Fig. 4A-C). However, in the hNPCs-grafted mice, which survived up to 30 weeks p.t., hNPCs generated similar proportions of APC^+ (87.1 ± 2.3%) and $NOGO\text{-}A^+$ (50.2 ± 5.3%) cells as hOPCs at 15 weeks p.t. (Fig. 4C), indicating their slower pace but equal capacity to differentiate into oligodendrocytes.

Grafted hNPCs and hOPCs differentiate into functional oligodendrocytes

Similarly, while myelin was detected in the majority of the structures colonized by grafted hOPCs at 15 weeks p.t., we only detected myelin-like debris in hNPCs-grafted mice, suggesting ongoing demyelination as observed in homozygous ungrafted mice (Fig. 5A). Consistent with their slower differentiation into mature oligodendrocytes, hNPCs achieved robust myelination only at 30 weeks p.t., with MBP^+ area in the corpus callosum (76.6 ± 19.7% of MBP^+ area) reaching similar extension to the one detected at 15 weeks p.t in hOPCs-grafted animals (64.7 ± 11.1%) (Fig. 5B-C). As MBP^+ myelin debris can persist in *Plp-tg:Rag* mice, we used multiple approaches to demonstrate that myelin was produced by the human grafted cells. First, orthogonal views of MBP^+ interactions with GFP^+ grafted cells

ScholarOne Support: (434) 964-4100

For Peer Review

revealed multiple branched processes ending in T shape, a typical feature of myelin-forming oligodendrocytes [13] connecting host axons (Fig. 5D). The myelinating potential of transplanted cells was further investigated by immuno-electron microscopy at 48 weeks p.t. BluoGal precipitates, which reveal GFP staining, were restricted to myelin structures and were exclusively present in areas containing GFP^+ cells prior to embedding. Therefore, detection of BluoGal precipitates by electron microscopy within myelin wrapping of host axons validated that myelin was donor derived (Fig. 5E). Higher magnification indicated that the donor-derived myelin was normally compacted. Finally, immunostaining for the paranodal protein Caspr and nodal Neurofascin revealed a higher density of nodes of Ranvier in areas of the corpus callosum containing GFP^+ cells compared to areas lacking GFP^+ cells or to ungrafted mice (Fig. 5F). Moreover, co-labeling for GFP and Caspr confirmed the donor origin of the paranodal structures (Fig. 5G). These data indicate nodal reconstitution by the gratfed cells and highlight the functionality of the donor-derived myelin.

Only grafted hNPCs down-regulate inflammation in Plp-tg:Rag mice

Despite their potential for efficient integration and myelination, hOPCs failed to improve the survival of *Plp-tg:Rag* mice. We therefore asked whether these two grafted cell populations might differentially modulate their host environment and in particular the inflammatory burden of *Plp-tg:Rag* mice. Indeed, *PLP1* overexpression leads to increased astrocytosis and massive microglial activation, both associated with aggravated clinical symptoms. We explored microglial and astrocyte reactivity in *Plp-tg:Rag* mice by immunodetection of Iba1 and GFAP respectively. Engraftment with hNPCs significantly reduced both microglial (Fig. 6A) and astrocyte (Fig. 6B) loads in white matter areas in *Plp-tg:Rag* as compared to ungrafted mice. The percentages of the corpus callosum labelled for GFAP and Iba1 were 49.1 ± 9.1% and 31.5 ± 2.4% respectively in ungrafted mice, 73.4 ± 17.4% and 39.0 ± 9.3%

ScholarOne Support: (434) 964-4100

For Peer Review

in hOPC-grafted mice and 18.6 ± 5.3% and 7.8 ± 1.2% in hNPCs-grafted mice. These data indicate reductions in astrocyte and microglial loads of ~3-4 fold in hNPCs-grafted animals compared to ungrafted and hOPC-grafted mice.

Different shapes and process ramifications of astrocytes and microglia in hOPCs- and hNPCs-grafted mice, prompted us to define the activation state of microglial cells. Classically activated (M1-like pro-inflammatory) and alternatively activated (M2-like repair associated) cells were identified by colocalization of either inducible nitric oxide synthase (iNOS; M1-like) or Arginase (Arg-1; M2-like) markers in $Iba1^+$ cells (Fig. 7A). While ungrafted mice were characterized by the exclusive presence of M1-type inflammatory phenotype, both hOPCs and hNPCs transplants tended to reduce the percentage of $Iba1^+/iNOS^+$ M1-like cells. While hOPCs sustained essentially M1-like microglial cell phenotype (48.1 ± 7.4% of $Iba1^+/iNOS^+$ cells versus 24.8 ± 2.6% of $Iba1^+/Arg\text{-}1^+$ M2-like cells), with a low M2/M1 ratio (0.51 ± 0.2), hNPCs induced a substantial shift from M1-like to M2-like phenotype (M2/M1 ratio =1.39 ± 0.12), with 35.3 ± 1.3% of $Iba1^+/iNOS^+$ and 49.0 ± 3.7% of $Iba1^+/Arg\text{-}1^+$ cells) (Fig. 7B). To further validate iNOS and Arginase expression levels as well as other M1-like (CD32, CD86, CD16) and M2-like (Tgfβ, CD206, Igf1) markers, we performed quantitative real-time RT-PCR on $CD11b^+$ cells, isolated from corpus callosum of hOPCs-, hNPCs-grafted mice and ungrafted mice. Analysis confirmed the trend for down-regulation of iNOS in both hNPCs- (0.66 ± 0.22) and hOPCs-grafted mice (0.14 ± 0.06) as well as higher expression of arginase in hNPCs-grafted mice (26.25 ± 3.14) compared to hOPCs-grafted mice (1.34 ± 0.67) (Fig. 7C). In parallel, the modulation of iNOS or arginase observed in hNPCs-grafted mice was correlated to results obtained *in vitro* with polarized microglia into the M1-like state by IFNγ, and into the M2-like phenotype by IL4 (iNOS: 0.36 ± 0.07; Arginase: 1,056.19 ± 21.76) normalized on unpolarised microglial cells (Fig. 7D). Thus exogenous hNPCs down-

ScholarOne Support: (434) 964-4100

For Peer Review

regulated the host inflammatory context more efficiently than hOPCs by polarizing $CD11b^{+}$ cells mainly into a repair M2-like state.

Discussion

PLP1 overexpression exerts a toxic gain-of-function resulting in oligodendrocyte death. Current endogenous repair strategies aim to minimize pathological effects of mutations using micro RNA to reduce Plp1 mRNA levels [28], or cholesterol treatment [29]. However, cell substitution may be another promising alternative therapy for PMD.

Proof of principle for cell-based therapy for PMD was provided by transplanting rodent CNS tissue fragments in *jimpy* mice [30], a PMD model of *Plp1* gene point-mutation, and was further confirmed by grafting purified populations of rodent glial precursor cells in myelin-deficient (md) rats [31] or shaking pups [32]. Although these studies demonstrated that non-affected rodent precursor cells survived and differentiated normally into oligodendrocytes in the PMD environment, the benefit of rodent NPCs or human NPCs/OPCs engraftment in these models has not been investigated. Moreover, rational progress with cell-therapy requires comparison of different cell types (NPCs versus OPCs) in the same experimental paradigm. Finally, in view of the obvious differences in biology existing between human and rodent cells, the efficacy of human cells in a relevant model of PMD has not been demonstrated but is required for appropriate clinical translation of cell therapy for PMD. In this study, we addressed whether hOPCs or hNPCs are better candidates for PMD cell-based therapy, by comparing these two populations in parallel after engraftment into the newborn brain of a mouse model of severe PMD.

Plp-tg mice were backcrossed with $Rag2^{-/-}$ littermates to prevent human cell rejection. Although previous studies have demonstrated the involvement of T-lymphocytes in myelin

ScholarOne Support: (434) 964-4100

For Peer Review

degeneration [33] and in the perturbation of retrograde axonal transport and axonal swelling in *Plp-tg* mice [34], we did not detect significant improvement of survival, disability, inflammation or myelination in *Plp-tg:Rag* mice compared to non-*Rag* littermates. Cells grafted rostrally to the corpus callosum of newborn pups migrated progressively into all brain regions, with a preference for areas controlling balance and motor coordination such as corpus callosum and *fimbria*. Rotarod data showed that motor coordination and balance of hNPCs-grafted *Plp-tg:Rag* mice was significantly improved compared to ungrafted *Plp-tg:Rag* mice at 25 weeks p.t., but was inferior to wild-type Rag-/- mice. Moreover, while rod fall latencies of *Plp-tg:Rag* mice decreased with time until death, that of hNPCs-grafted mice remained higher over time. This mild improvement might result from newly formed myelin, in areas involved in locomotion/balance, such as the cerebellum. Possibly, transplanting more cells or targeting more sites [18] might optimize cell spreading to the cerebellum, brainstem and spinal cord and further improve locomotor activity and survival.

Several studies highlighted that transplantation of hOPCs, derived from foetal brain or from iPS, into immunodeficient *shiverer:Rag* mouse brain induced widespread myelination and extended lifespan of their host [17, 18]. Surprisingly, this was not the case when hOPCs were grafted into *Plp-tg:Rag* mice. In spite of the presence of extensive exogenous myelination, hOPCs-grafted mice died as prematurely as ungrafted mice (20 weeks). The failure of hOPCs to promote *Plp-tg:Rag* survival was not due to any potential intrinsic defect of the grafted hOPCs population. Indeed, these hNPCs-derived hOPCs were bonified hOPCs expressing OPCs markers such as PDGFRα and Olig2, as validated at the protein and transcriptional levels. Second, after engraftment into immunodeficient *shiverer:Rag* mice, grafted hOPCs differentiated successfully into myelin-forming cells and improved host survival, from 23 to 30 weeks (Fig. 2J) as previously reported [17]. Additionally, their failure to improve *Plp-*

ScholarOne Support: (434) 964-4100

For Peer Review

tg:Rag mice survival did not result from excessive cell death since hOPCs did not express Caspase 3 and were present in equal densities to hNPCs after engraftment in the *Plp-tg:Rag* cerebral parenchyme. The absence of rescue of the *Plp-tg:Rag* phenotype in spite of exogenous hOPCs-derived myelination highlights the existence of a major pathological process, which is linked preferentially to inflammation rather than demyelination. The significance of the inflammatory process is reinforced by the unexpected improvement of hNPCs-grafted mice survival up to one year p.t., in spite of the absence of myelination at 15 weeks p.t. This extended survival following hNPCs transplantation may result from hNPCs-derived immunomodulation since astrocyte reactivity and microglial density were reduced at 15 weeks p.t. Reduction of the inflammatory burden allowed the slow process of differentiation of hNPCs into oligodendrocytes to proceed beyond the otherwise restricted lifespan of their host. The observation that hNPCs and hOPCs extend survival of *shiverer:Rag* mice but that only hNPCs increase life expectancy of *Plp-tg:Rag* mice, suggests that a mildly inflammatory phenotype such as *shiverer* can be rescued by myelination [35] while a severe inflammatory PMD phenotype requires efficient immunomodulation in addition to myelin restoration. Moreover, the difference in survival between these two models highlights the limits of the *shiverer* model [26] and the necessity to use more relevant disease models, such as *Plp-tg:Rag* mice, to develop efficient cell therapy for PMD.

Unlike in *shiverer* mice [13], hNPCs transplanted into *Plp-tg:Rag* animals differentiated predominantly into oligodendrocytes but to a minor extent into astrocytes or neurons, suggesting that disease-specific environments affect differentially the fate of exogenous cells. Therefore, it seems that therapeutic strategies using hOPCs with astrocytes or neurons cannot be efficient in PMD. It also highlights that the major difference in the respective therapeutic benefits between hNPCs and hOPCs results more from mechanisms such as modulation of inflammation rather than the myelination capacities of the two populations. Although hNPCs

For Peer Review

ScholarOne Support: (434) 964-4100

required twice more time than hOPCs to generate mature oligodendrocytes, both cell types were equally myelinogenic, producing robust myelination in their target sites, as validated by immunodetection of GFP by fluorescent and electron microscopy. Moreover, hNPCs grafted in newborn *shiverer:Rag* mice differentiated along the same time frame as in *Plp-tg:Rag* mice, indicating that the PMD environment neither prevented [30] nor delayed the maturation of healthy exogenous cells.

Both hNPCs and hOPCs migrated widely with a preference for white matter tracks. Widespread white matter colonization by the grafted cells suggests strong chemoattractive signalling, possibly mediated via M1-like microglial cells [36] which are present in *Plp-tg:Rag* white matter. Interestingly, only hNPCs reduced microglial cell number and astrocyte reactivity, confirming the anti-inflammatory properties of NPCs as revealed after intravenous or intraparenchymal injection [21, 24, 25], and highlighting that this effect is sustained irrespective of the disease inflammatory context.

The presence of hNPCs in *Plp-tg:Rag* mice was associated with a switch of M1-like microglial cells phenotype into M2-like anti-inflammatory cells phenotype, and suggests the release of immunomodulatory factors as observed for mouse-NPCs grafted in the injured spinal cord [25] or during endogenous remyelination [36]. Although iNOS transcript expression level was lower in hOPCs-transplanted mice than in hNPCs-grafted mice, microglial cells remained essentially M1-like. This presumably results from insufficiency or a different spectrum of secreted trophic factors and cytokines involved in M2-like polarization as suggested by the weak expression of arginase and other M2-like markers. Rescue of hNPCs-grafted *Plp-tg:Rag* mice could result from the modification of M1/M2 balance rather than the decrease of microglial cell number as observed in Krabbe's disease [37]. Thus, the different response of hNPCs and hOPCs on *Plp-tg:Rag* mice inflammation highlights their respective immunomodulatory properties through their own spectrum of secreted cytokines.

For Peer Review

ScholarOne Support: (434) 964-4100

Deciphering how hNPCs mediate the transition from M1-like to M2-like phenotype in *Plp-tg:Rag* mice could lead to the identification of therapeutic molecules and further improve PMD cell therapy [38]. Indeed, a strategy combining pharmacological immunomodulation to improve recipient survival and fast and efficient myelin replacement via cell therapy to prevent axon dysfunction would appear as an optimal therapeutic treatment for PMD and possibly other inflammatory demyelinating disorders. Indeed, although this study highlights the benefit of hNPCs transplantation in a severe PMD model, the optimal strategy could be to accelerate the generation of myelin to protect axons using hOPCs in combination with the use of immunomodulatory drugs to reduce the deleterious effect of inflammation. One could question the relevance of our data on microglia phenotype in PMD. Indeed, very few histopathological studies reported inflammation in PMD and none of them described microglial polarization. Although, recent data indicated microglial activation in a variety of PMD patients, including those affected with *PLP1* duplication [5], histopathological data are insufficient to infer whether inflammation precedes or results from demyelination. In the latter case, it could aggravate PMD physiopathology. Interestingly and even more relevant to the human disease is the effect of hNPCs on astrocytosis which is commonly described in PMD [39]. As astrocytes and microglia may be activated by each other [40-42], it remains plausible that the observed effects on microglia are mediated via astrocytes or vice-versa.

Conclusion

In summary, we provide the first evidence that immunomodulation, myelin repair and clinical improvement can be successfully achieved by hNPCs cell therapy in a model of severe PMD. Our work highlights the major role of neuroinflammation (microglial activation and astrocytosis) in disease severity and the link between successful modulation of this parameter and *Plp-tg_Rag* mice lifespan. Finally and unexpectedly, we found that exogenous hNPCs

ScholarOne Support: (434) 964-4100

For Peer Review

restrained more efficiently the severe murine PMD phenotype by providing first immunomodulation and second myelin repair. Although future studies should elucidate the molecular and cellular events underlying down-regulation of neuroinflammation and neuroprotection provided by hNPCs in experimental PMD, our present findings may pave the way to optimize cell-based therapies for myelin disorders associated with progressive inflammation.

Acknowledgments

The authors wish to thank the CYPS Flow Cytometry and PICPS Cellular Imaging facilities of the Pitié-Salpêtrière site, the neuroimaging (CENIR), cell imaging, histology, cell culture, genotyping and sequencing, and rodent behaviour core facilities of ICM. The author would like to thank Dr. Teresa Wood of the New Jersey Medical School for comments, suggestions and help with editing of the manuscript.

This work was supported by the European Leukotreat project # FP7-Health-F2-2100-241622, the European Foundation for Leukodystrophies (ELA) 2010-003C5A, the "Institut pour la Recherche sur la Moelle épinière et l'Encéphale" (IRME), the "ICM Carnot Institut", the program "Investissements d'Avenir" ANR-10-IAIHU-06 and "Translational Research Infrastructure for Biotherapies in Neurosciences" ANR-11-INBS-0011–NeurATRIS.

Disclosure of potential Conflicts of interest: The authors declare no conflict of interest.

For Peer Review

ScholarOne Support: (434) 964-4100

References

1. Bachstetter AD, Webster SJ, Van Eldik LJ *et al*: Clinically relevant intronic splicing enhancer mutation in myelin proteolipid protein leads to progressive microglia and astrocyte activation in white and gray matter regions of the brain. *J Neuroinflammation* 2013, 10:146.
2. Bradl M, Bauer J, Inomata T *et al*: Transgenic Lewis rats overexpressing the proteolipid protein gene: myelin degeneration and its effect on T cell-mediated experimental autoimmune encephalomyelitis. *Acta Neuropathol* 1999, 97(6):595-606.
3. Tatar CL, Appikatla S, Bessert DA *et al*: Increased Plp1 gene expression leads to massive microglial cell activation and inflammation throughout the brain. *ASN Neuro* 2010, 2(4):e00043.
4. Gorman MP, Golomb MR, Walsh LE *et al*: Steroid-responsive neurologic relapses in a child with a proteolipid protein-1 mutation. *Neurology* 2007, 68(16):1305-1307.
5. Southwood CM, Fykkolodziej B, Dachet F *et al*: Potential For Cell-mediated Immune Responses In Mouse Models Of Pelizaeus-Merzbacher Disease. *Brain Sci* 2013, 3(4):1417-1444.
6. Mimault C, Giraud G, Courtois V *et al*: Proteolipoprotein gene analysis in 82 patients with sporadic Pelizaeus-Merzbacher Disease: duplications, the major cause of the disease, originate more frequently in male germ cells, but point mutations do not. The Clinical European Network on Brain Dysmyelinating Disease. *Am J Hum Genet* 1999, 65(2):360-369.
7. Readhead C, Schneider A, Griffiths I *et al*: Premature arrest of myelin formation in transgenic mice with increased proteolipid protein gene dosage. *Neuron* 1994, 12(3):583-595.
8. Gow A, Friedrich VL, Jr., Lazzarini RA: Intracellular transport and sorting of the oligodendrocyte transmembrane proteolipid protein. *J Neurosci Res* 1994, 37(5):563-573.
9. Southwood CM, Garbern J, Jiang W *et al*: The unfolded protein response modulates disease severity in Pelizaeus-Merzbacher disease. *Neuron* 2002, 36(4):585-596.
10. Clark K, Sakowski L, Sperle K *et al*: Gait abnormalities and progressive myelin degeneration in a new murine model of Pelizaeus-Merzbacher disease with tandem genomic duplication. *J Neurosci* 2013, 33(29):11788-11799.
11. Cremers FP, Pfeiffer RA, van de Pol TJ *et al*: An interstitial duplication of the X chromosome in a male allows physical fine mapping of probes from the Xq13-q22 region. *Hum Genet* 1987, 77(1):23-27.
12. Garbern JY: Pelizaeus-Merzbacher disease: pathogenic mechanisms and insights into the roles of proteolipid protein 1 in the nervous system. *J Neurol Sci* 2005, 228(2):201-203.
13. Buchet D, Garcia C, Deboux C *et al*: Human neural progenitors from different foetal forebrain regions remyelinate the adult mouse spinal cord. *Brain* 2011, 134(Pt 4):1168-1183.
14. Uchida N, Chen K, Dohse M *et al*: Human neural stem cells induce functional myelination in mice with severe dysmyelination. *Sci Transl Med* 2012, 4(155):155ra136.
15. Sim FJ, McClain CR, Schanz SJ *et al*: CD140a identifies a population of highly myelinogenic, migration-competent and efficiently engrafting human oligodendrocyte progenitor cells. *Nat Biotechnol* 2011, 29(10):934-941.

For Peer Review

ScholarOne Support: (434) 964-4100

16. Windrem MS, Nunes MC, Rashbaum WK *et al*: Fetal and adult human oligodendrocyte progenitor cell isolates myelinate the congenitally dysmyelinated brain. *Nat Med* 2004, 10(1):93-97.
17. Wang S, Bates J, Li X *et al*: Human iPSC-derived oligodendrocyte progenitor cells can myelinate and rescue a mouse model of congenital hypomyelination. *Cell Stem Cell* 2013, 12(2):252-264.
18. Windrem MS, Schanz SJ, Guo M *et al*: Neonatal chimerization with human glial progenitor cells can both remyelinate and rescue the otherwise lethally hypomyelinated shiverer mouse. *Cell Stem Cell* 2008, 2(6):553-565.
19. Goldman SA, Nedergaard M, Windrem MS: Glial progenitor cell-based treatment and modeling of neurological disease. *Science* 2012, 338(6106):491-495.
20. Goldman SA, Windrem MS: Cell replacement therapy in neurological disease. *Philos Trans R Soc Lond B Biol Sci* 2006, 361(1473):1463-1475.
21. Einstein O, Grigoriadis N, Mizrachi-Kol R *et al*: Transplanted neural precursor cells reduce brain inflammation to attenuate chronic experimental autoimmune encephalomyelitis. *Exp Neurol* 2006, 198(2):275-284.
22. Laterza C, Merlini A, De Feo D *et al*: iPSC-derived neural precursors exert a neuroprotective role in immune-mediated demyelination via the secretion of LIF. *Nat Commun* 2013, 4:2597.
23. Pluchino S, Gritti A, Blezer E *et al*: Human neural stem cells ameliorate autoimmune encephalomyelitis in non-human primates. *Ann Neurol* 2009, 66(3):343-354.
24. Pluchino S, Quattrini A, Brambilla E *et al*: Injection of adult neurospheres induces recovery in a chronic model of multiple sclerosis. *Nature* 2003, 422(6933):688-694.
25. Cusimano M, Biziato D, Brambilla E *et al*: Transplanted neural stem/precursor cells instruct phagocytes and reduce secondary tissue damage in the injured spinal cord. *Brain* 2012, 135(Pt 2):447-460.
26. Trapp BD: Rescue of congenital hypomyelination by progenitor cell transplantation. *Cell Stem Cell* 2008, 2(6):519-520.
27. Chhor V, Le Charpentier T, Lebon S *et al*: Characterization of phenotype markers and neuronotoxic potential of polarised primary microglia in vitro. *Brain Behav Immun* 2013, 32:70-85.
28. Prukop T, Epplen DB, Nientiedt T *et al*: Progesterone antagonist therapy in a Pelizaeus-Merzbacher mouse model. *Am J Hum Genet* 2014, 94(4):533-546.
29. Saher G, Rudolphi F, Corthals K *et al*: Therapy of Pelizaeus-Merzbacher disease in mice by feeding a cholesterol-enriched diet. *Nat Med* 2012, 18(7):1130-1135.
30. Lachapelle F, Lapie P, Nussbaum JL *et al*: Immunohistochemical studies on cross-transplantations between jimpy, shiverer, and normal newborn mice. *J Neurosci Res* 1990, 27(3):324-331.
31. Brustle O, Jones KN, Learish RD *et al*: Embryonic stem cell-derived glial precursors: a source of myelinating transplants. *Science* 1999, 285(5428):754-756.
32. Archer DR, Cuddon PA, Lipsitz D *et al*: Myelination of the canine central nervous system by glial cell transplantation: a model for repair of human myelin disease. *Nat Med* 1997, 3(1):54-59.
33. Ip CW, Kroner A, Bendszus M *et al*: Immune cells contribute to myelin degeneration and axonopathic changes in mice overexpressing proteolipid protein in oligodendrocytes. *J Neurosci* 2006, 26(31):8206-8216.
34. Ip CW, Kroner A, Groh J *et al*: Neuroinflammation by cytotoxic T-lymphocytes impairs retrograde axonal transport in an oligodendrocyte mutant mouse. *PLoS One* 2012, 7(8):e42554.

For Peer Review

ScholarOne Support: (434) 964-4100

35. Chen H, Cabon F, Sun P *et al*: Regional and developmental variations of GFAP and actin mRNA levels in the CNS of jimpy and shiverer mutant mice. *J Mol Neurosci* 1993, 4(2):89-96.
36. Miron VE, Boyd A, Zhao JW *et al*: M2 microglia and macrophages drive oligodendrocyte differentiation during CNS remyelination. *Nat Neurosci* 2013, 16(9):1211-1218.
37. Kondo Y, Adams JM, Vanier MT *et al*: Macrophages counteract demyelination in a mouse model of globoid cell leukodystrophy. *J Neurosci* 2011, 31(10):3610-3624.
38. Gupta N, Henry RG, Strober J *et al*: Neural stem cell engraftment and myelination in the human brain. *Sci Transl Med* 2012, 4(155):155ra137.
39. Sima AA, Pierson CR, Woltjer RL *et al*: Neuronal loss in Pelizaeus-Merzbacher disease differs in various mutations of the proteolipid protein 1. *Acta Neuropathol* 2009, 118(4):531-539.
40. Abudara V, Roux L, Dallerac G *et al*: Activated microglia impairs neuroglial interaction by opening Cx43 hemichannels in hippocampal astrocytes. *Glia* 2015.
41. Mayo L, Quintana FJ, Weiner HL: The innate immune system in demyelinating disease. *Immunol Rev* 2012, 248(1):170-187.
42. Mayo L, Trauger SA, Blain M *et al*: Regulation of astrocyte activation by glycolipids drives chronic CNS inflammation. *Nat Med* 2014, 20(10):1147-1156.

For Peer Review

Figure Legends:

Figure 1. Characterization of adult *Plp-tg:Rag* mice.

Hypomyelination of homozygous *Plp-tg:Rag* mice compared to wild-type mice is revealed by electron microscopy **(A)**, MRI scans **(B)**, and immunohistochemistry for MBP (red) **(C, C')**. Astrocytosis **(D, D')** and microglial activation **(E, E')** are detected respectively by GFAP (red) and Iba1 (red) immunolabeling (n=3 per group). Nuclei are counterstained by Dapi (blue). cc: corpus callosum; f: *fimbria*; v: lateral ventricle. Scale bars: (A) 1 µm; (C-E) 100 µm; (C'-E') 500 µm.

Figure 2. Phenotype of CD140a sorted cells.

Both CD140a-PE positive and negative fraction were characterized 24hrs after sorting. The positive fraction expressed **(A)** the OPC marker PDGFR alpha, **(B)** the oligodendroglial lineage transcription factor Olig2 and **(C)** the proliferation marker Ki67. The negative fraction did not express **(D)** PDGFR alpha or **(E)** Olig2. **(F)** Most of this population was neuronal,

ScholarOne Support: (434) 964-4100

expressing TuJI. Scale bars: 50 µm. **(G)** Quantitative RT-PCR highlighted gene set enrichment of both positive (green) and negative (red) fractions. Data (n = 4) are presented as values of total cell population before sorting after normalization with Cyclophilin A levels. **(H-I)** Horizontal sections through the corpus callosum of a 15 week old shiverer:Rag mice demonstrated that **(H)** CD140a-sorted hOPCs myelinate more effectively than **(I)** hNPCs. **(J)** Shiverer:Rag mice transplanted with CD140a-sorted hOPCs survived up to 30 weeks. MBP is stained in red, GFP^+ cells are in green. $Dapi^+$ nuclei are in blue. Scale bars: (H-J) 800 µm; (H'-J') 200 µm.

Figure 3. hNPCs grafted mice exhibit increased lifespan and locomotor improvement.

(A) Kaplan-Meier survival graph and **(B)** histogram showing the percentage of hNPCs-(n=27), hOPCs-grafted mice (n=11) and ungrafted (Ug) mice surviving (n=76) with age. (+) corresponds to mice sacrificed for immunochemistry or electron microscopy. **(C)** Latency to fall (sec) monitored by accelerating rotarod assay. $Rag2^{-/-}$ mice were used for controls (n=6). Results are the mean of three consecutive tests. The curves of hOPCs-grafted mice and ungrafted mice stop respectively at 15 and 30 weeks p.t. because of their premature death. Error bars indicate ± SEM. *p < 0.05; **p<0.01; ***p<0.001 versus the indicated groups using Student's t test.

Figure 4. hNPCs and hOPCs give rise to mature oligodendrocytes after transplantation into the corpus callosum of *Plp-tg:Rag* mice.

Double immunohistochemical labeling for GFP (green) and human specific NOGO-A (red) **(A)** or APC (red) **(B)** reveal differentiation of hOPCs (n=3) and hNPCs (15 weeks: n=3; 30 weeks: n=4) into mature oligodendrocytes in *Plp-tg:Rag* mice (arrows). Nuclei are counterstained by Dapi (blue). Scale bars represent 50 µm. **(C)** Quantification of the

ScholarOne Support: (434) 964-4100

For Peer Review

percentage of APC$^+$ or NOGO-A$^+$ cells on the total number of GFP$^+$ cells. Data are shown as mean ± SEM. *p < 0.05; **p<0.01; ***p<0.001 versus the indicated groups using Student's t test.

Figure 5. hOPCs and hNPCs produce myelin and restore nodes of Ranvier after transplantation in *Plp-tg:Rag* mice.

(A, B) Horizontal sections through the corpus callosum illustrating substantial remyelination by hOPCs at 15 weeks **(A)** and hNPCs at 30 weeks **(B)**. **(C)** Quantification of myelin corresponds to the percentage of MBP labelled area of the corpus callosum. (ungrafted: n=3; hOPCs: n=3; hNPCs: 15 weeks n=5; 30 weeks n=3). Data are shown as mean ± SEM. **(D)** Orthogonal projection of hNPCs in contact with myelin internodes (arrows) and **(E)** presence of Bluo-gal precipitates in myelin sheaths enwrapping axons demonstrate donor-derived myelination. MBP is stained in red, GFP$^+$ cells are in green. Dapi$^+$ nuclei are in blue. **(F)** Nodal reconstitution by hOPCs and hNPCs-derived oligodendrocytes is revealed by immunostaining of paranodal Caspr (red) and nodal Neurofascin (green) proteins. **(G)** Involvement of both type of grafted cells in nodal reconstitution is reported by immunostaining of paranodal Caspr (red) and GFP (green) proteins. Dapi$^+$ nuclei are in blue. Lower panels in (A) and (B) are higher magnifications of top panels. cc: corpus callosum; f: *fimbria*; v: lateral ventricle. Scale bars: (A-B) 100 µm higher panel, 25 µm lower panel; (D) 500 µm; (E) 200 nm; (F-G) 5 µm. *p < 0.05; **p<0.01; ***p<0.001 versus the indicated groups using Student's t test.

Figure 6. Human hNPCs down-regulate microglia and astrocyte loads.

(A, B) Microglial cells **(A)** and astrocytes **(B)** load at 15 weeks p.t. Microglial cells (Iba1) and astrocytes (GFAP) are stained in red while human cells (GFP) are in green, Dapi$^+$ nuclei are

ScholarOne Support: (434) 964-4100

For Peer Review

in blue. Lower panels of (A) and (B) are higher magnifications of top panels. Scale bars: 100 µm higher panel, 25 µm lower panel. **(C, D)** Quantification of microglia **(C)** and astrocyte **(D)** densities are expressed as the percentage of Iba1 and GFAP labelled areas of the corpus callosum (ungrafted: n=3; hOPCs: n=3; hNPCs: n=9). Data are shown as mean ± SEM. *p < 0.05; **p<0.01; ***p<0.001 versus the indicated groups using Student's t test.

Figure 7. Human hNPCs induce a M2-like microglial phenotype.

(A) M1-like and M2-like microglia activation state are revealed by colocalization of $Iba1^+$ cells (green) with iNOS or Arginase-1 (red) respectively. $Dapi^+$ nuclei are in blue. The flat morphology in the ungrafted and hOPCs-grafted mice correlates with the $iNOS^+$ M1-like activated state while the bipolar morphology of microglia in hNPCs-grafted mice correlates with the Arginase-1 M2-like state (ungrafted: n=3; hOPCs: n=3; hNPCs: n=9). Scale bars represent 50 µm. **(B)** Ratio of the percentage of $Iba1^+/Arg\text{-}1^+$ cells (M2-like) to the percentage of $Iba1^+/iNOS^+$ cells (M1-like). **(C-D)** Quantitative real-time RT-PCR highlighted modulation of classically activated M1-like and alternatively activated M2-like gene expression of **(C)** $CD11b^+$ cells isolated from hNPCs- and hOPCs-grafted mice versus $CD11b^+$ cells from ungrafted mice, and of **(D)** *in vitro* IL-4-atcivated or IFNγ-activated microglial cell versus unactivated microglia. Data are presented as values of relative gene expression after normalization with GAPDH levels. Data are shown as mean ± SEM. *p < 0.05; **p<0.01; ***p<0.001 versus the indicated groups using Student's t test.

For Peer Review

ScholarOne Support: (434) 964-4100

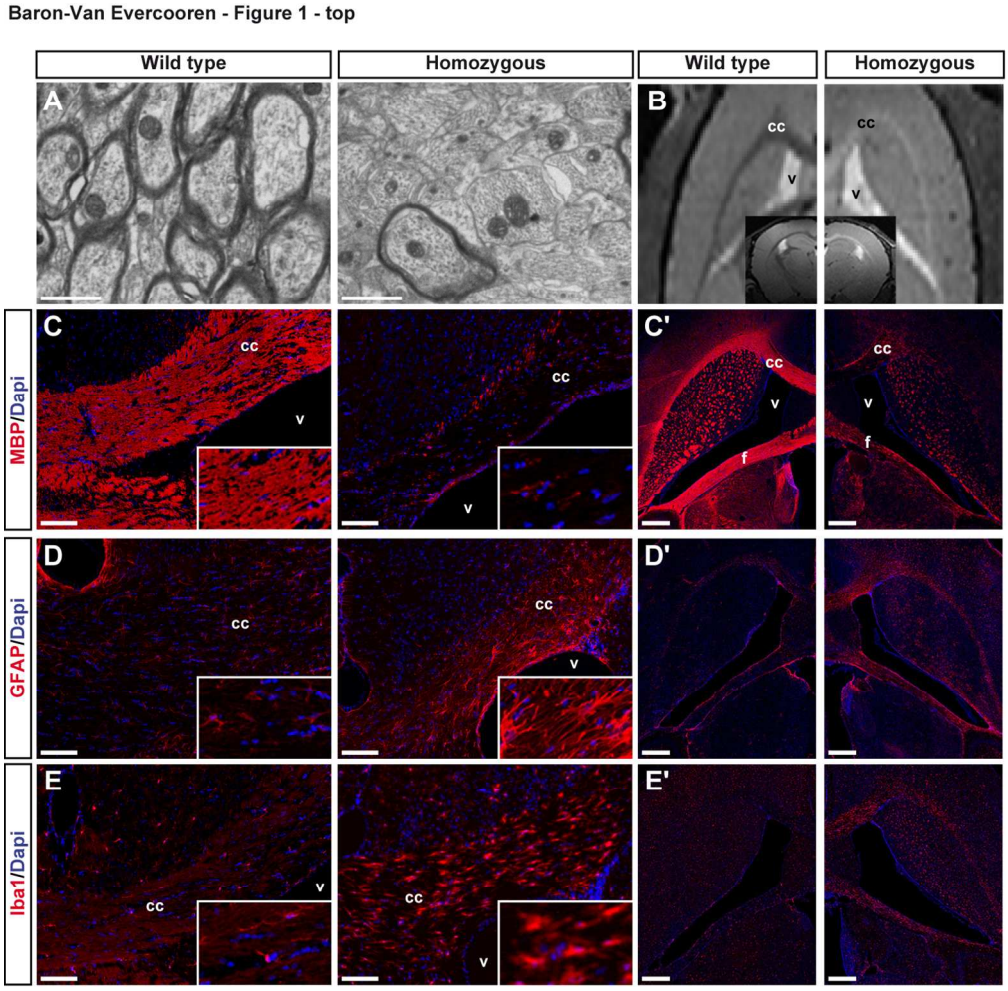

Figure 1. Characterization of adult Plp-tg:Rag mice.
Hypomyelination of homozygous Plp-tg:Rag mice compared to wild-type mice is revealed by electron microscopy (A), MRI scans (B), and immunohistochemistry for MBP (red) (C, C'). Astrocytosis (D, D') and microglial activation (E, E') are detected respectively by GFAP (red) and Iba1 (red) immunolabeling (n=3 per group). Nuclei are counterstained by Dapi (blue). cc: corpus callosum; f: fimbria; v: lateral ventricle. Scale bars: (A) 1 µm; (C-E) 100 µm; (C'-E') 500 µm.
128x126mm (300 x 300 DPI)

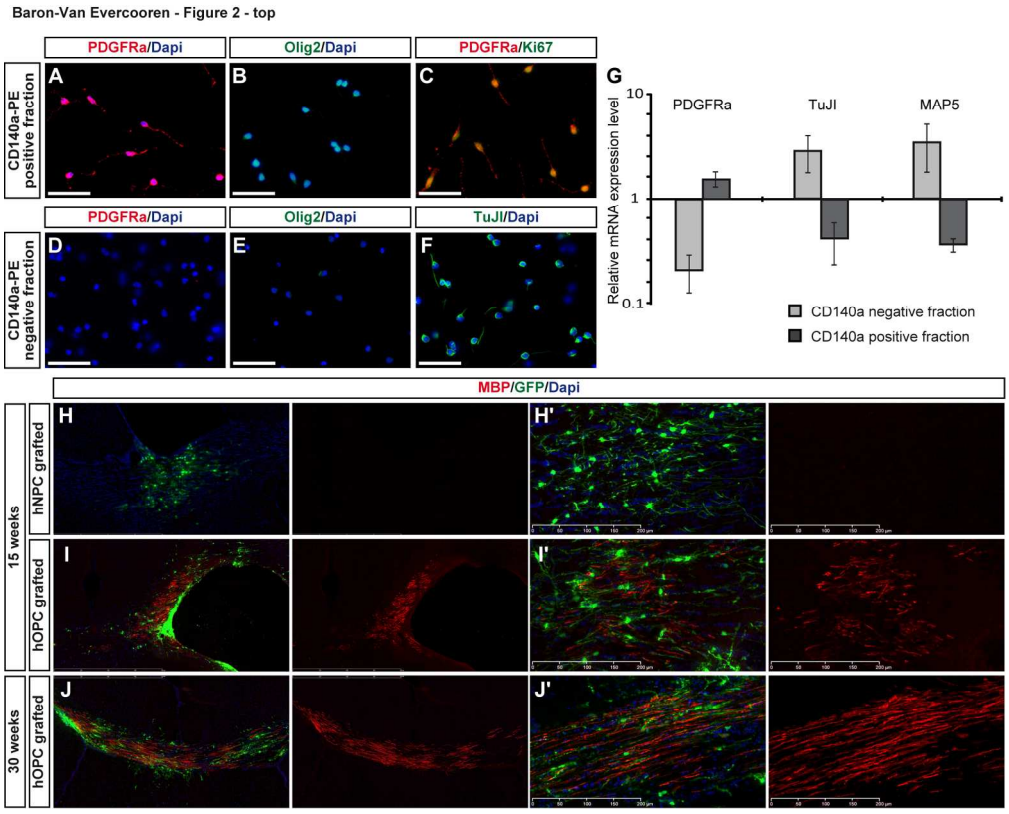

Figure 2. Phenotype of CD140a sorted cells.
24hrs after sorting, both CD140a-PE positive and negative fraction were characterized. Positive fraction expressed (A) the OPC marker PDGFR alpha, (B) the oligodendroglial lineage transcription factor Olig2 and (C) the proliferation marker Ki67. Negative fraction did not express (D) PDGFR alpha or (E) Olig2. (F) Most of this population was neuronal, expressing TuJI. Scale bars: 50 μm. (G) Quantitative real-time RT-PCR highlighted gene set enrichment of both positive (green) and negative (red) fraction. Data (n = 4) are presented as values of total cell population before sorting after normalization with Cyclophilin A levels. (H-I) Horizontal sections through the corpus callosum of a 15 week old shiverer:Rag mice demonstrated that (H) CD140a-sorted hOPCs myelinate more effectively than (I) hNPCs. (J) Shiverer:Rag mice transplanted with CD140a-sorted hOPCs survived up to 30 weeks. MBP is stained in red, GFP+ cells are in green. Dapi+ nuclei are in blue. Scale bars: (H-J) 800 μm; (H'-J') 200 μm.

169x136mm (300 x 300 DPI)

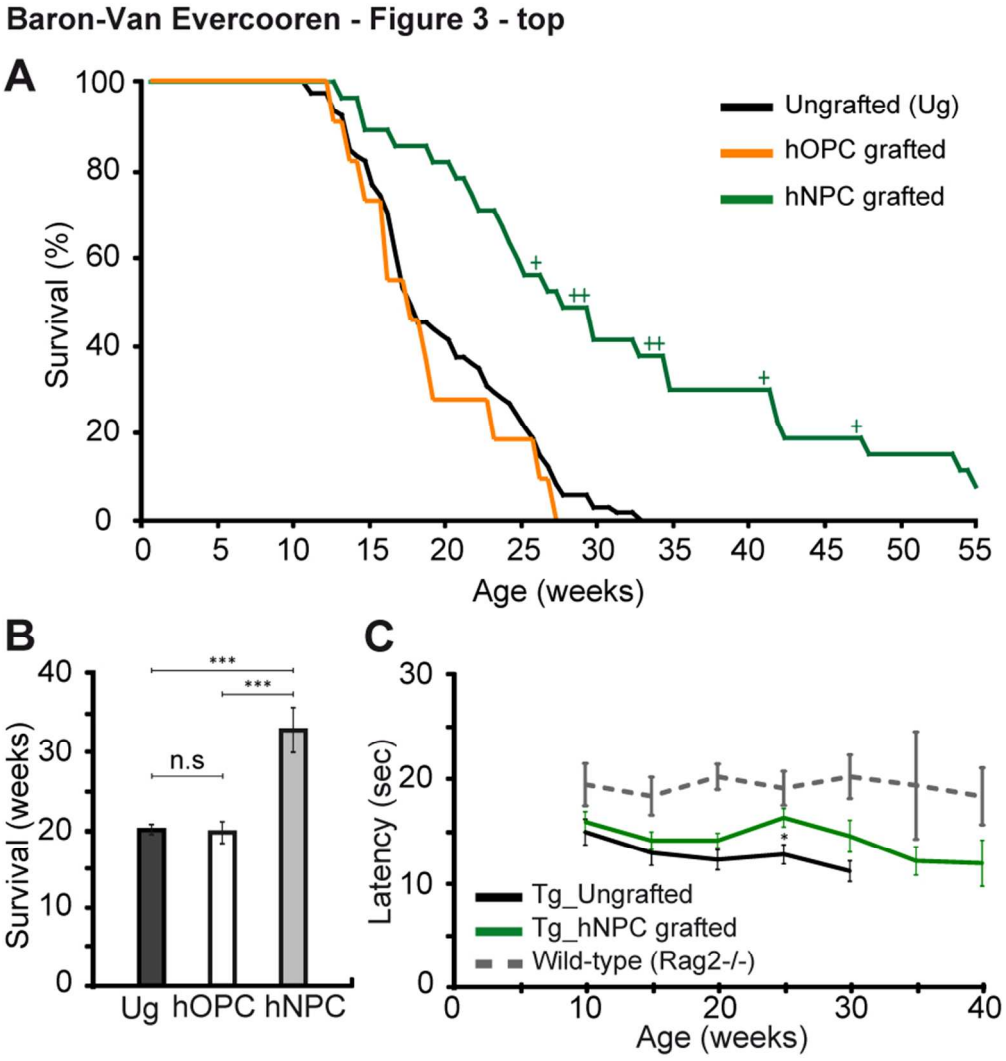

Figure 3. hNPCs grafted mice exhibit increased lifespan and locomotor improvement.
(A) Kaplan-Meier survival graph and (B) histogram showing the percentage of hNPCs- (n=27), hOPCs-grafted mice (n=11) and ungrafted (Ug) mice surviving (n=76) with age. (+) corresponds to mice sacrificed for immunochemistry or electron microscopy. (C) Latency to fall (sec) monitored by accelerating rotarod assay. Rag2-/- mice were used for controls (n=6). Results are the mean of three consecutive tests. The curves of hOPCs-grafted mice and ungrafted mice stop respectively at 15 and 30 weeks p.t. because of their premature death. Error bars indicate ± SEM. *p < 0.05; **p<0.01; ***p<0.001 versus the indicated groups using Student's t test.
80x84mm (300 x 300 DPI)

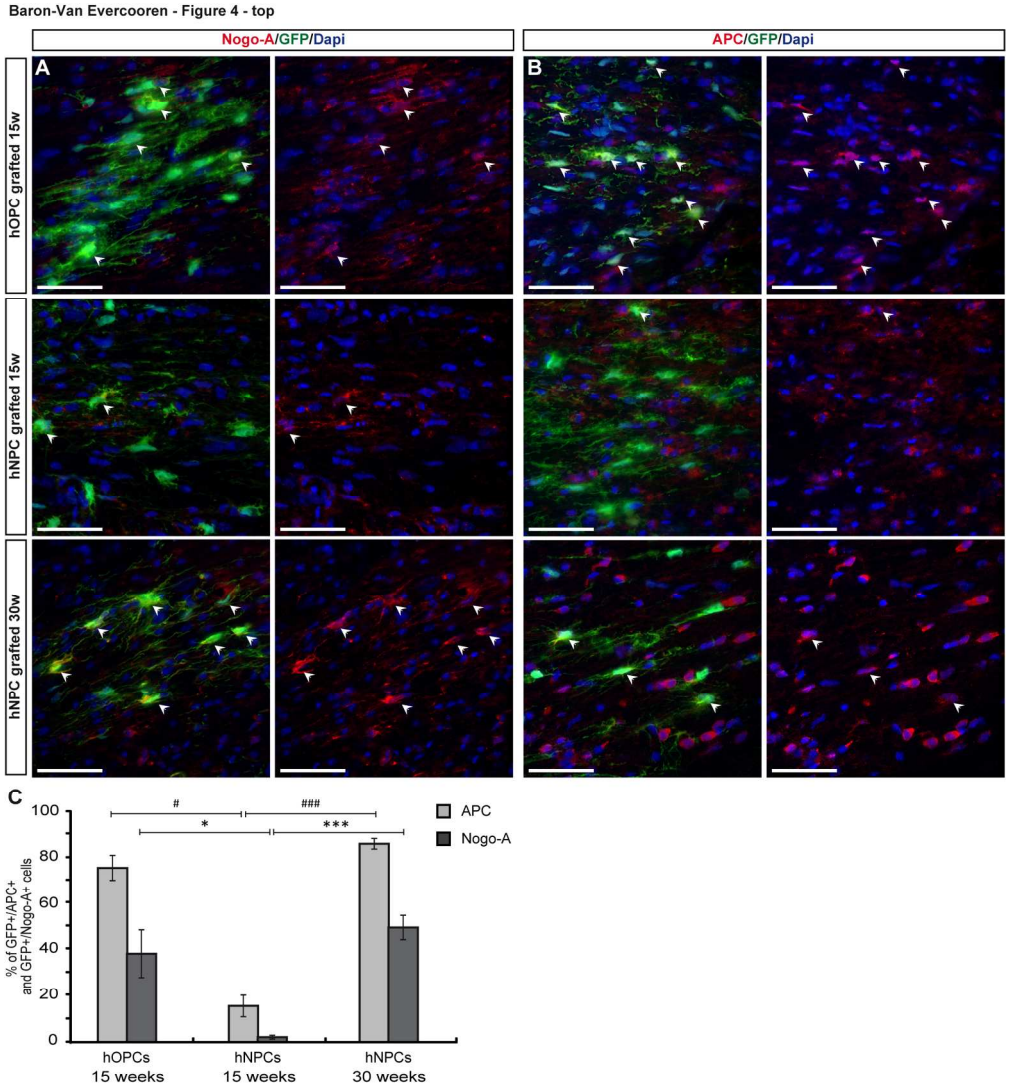

Figure 4. hNPCs and hOPCs give rise to mature oligodendrocytes after transplantation into the corpus callosum of Plp-tg:Rag mice.
Double immunohistochemical labeling for GFP (green) and human specific NOGO-A (red) (A) or APC (red) (B) reveal differentiation of hOPCs (n=3) and hNPCs (15 weeks: n=3; 30 weeks: n=4) into mature oligodendrocytes in Plp-tg:Rag mice (arrows). Nuclei are counterstained by Dapi (blue). Scale bars represent 50 µm. (C) Quantification of the percentage of APC+ or NOGO-A+ cells on the total number of GFP+ cells. Data are shown as mean ± SEM. *p < 0.05; **p<0.01; ***p<0.001 versus the indicated groups using Student's t test.

168x182mm (300 x 300 DPI)

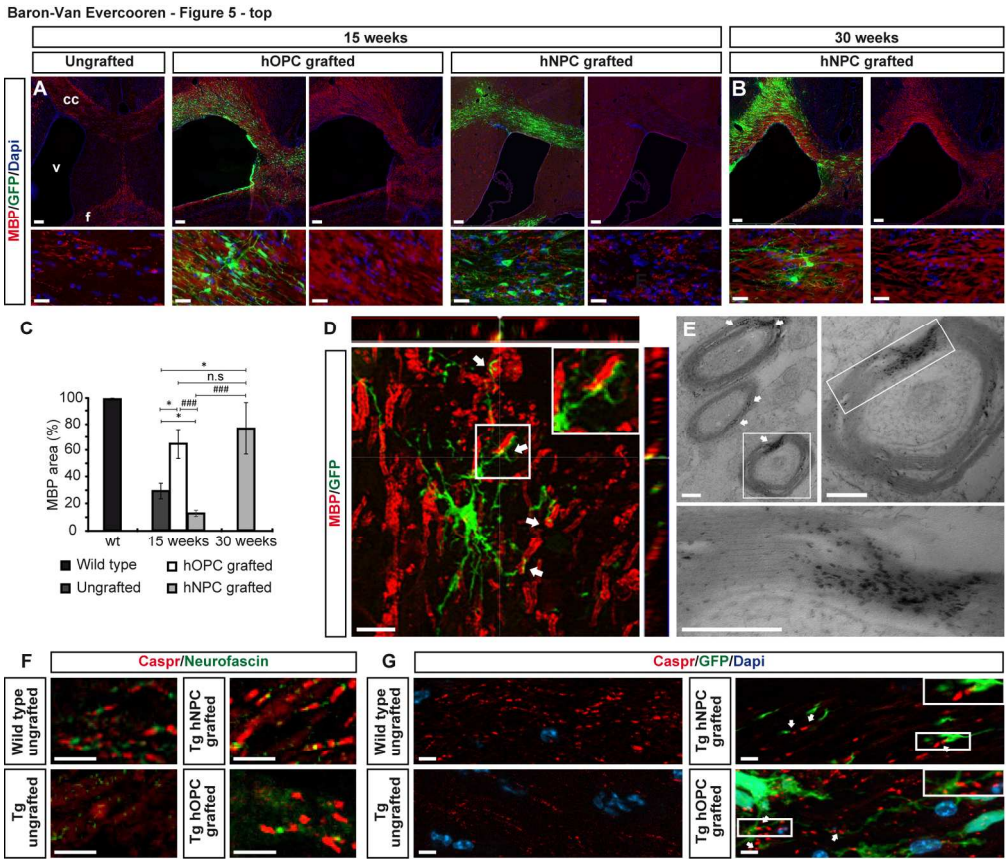

Figure 5. hOPCs and hNPCs produce myelin and restore nodes of Ranvier after transplantation in Plp-tg:Rag mice.

(A, B) Horizontal sections through the corpus callosum illustrating substantial remyelination by hOPCs at 15 weeks (A) and hNPCs at 30 weeks (B). (C) Quantification of myelin corresponds to the percentage of MBP labelled area of the corpus callosum. (ungrafted: n=3; hOPCs: n=3; hNPCs: 15 weeks n=5; 30 weeks n=3). Data are shown as mean ± SEM. (D) Orthogonal projection of hNPCs in contact with myelin internodes (arrows) and (E) presence of Bluo-gal precipitates in myelin sheaths enwrapping axons demonstrate donor-derived myelination. MBP is stained in red, GFP+ cells are in green. Dapi+ nuclei are in blue. (F) Nodal reconstitution by hOPCs and hNPCs-derived oligodendrocytes is revealed by immunostaining of paranodal Caspr (red) and nodal Neurofascin (green) proteins. (G) Involvement of both type of grafted cells in nodal reconstitution is reported by immunostaining of paranodal Caspr (red) and GFP (green) proteins. Dapi+ nuclei are in blue. Lower panels in (A) and (B) are higher magnifications of top panels. cc: corpus callosum; f: fimbria; v: lateral ventricle. Scale bars: (A-B) 100 µm higher panel, 25 µm lower panel; (D) 500 µm; (E) 200 nm; (F-G) 5 µm. *p < 0.05; **p<0.01; ***p<0.001 versus the indicated groups using Student's t test.
169x144mm (300 x 300 DPI)

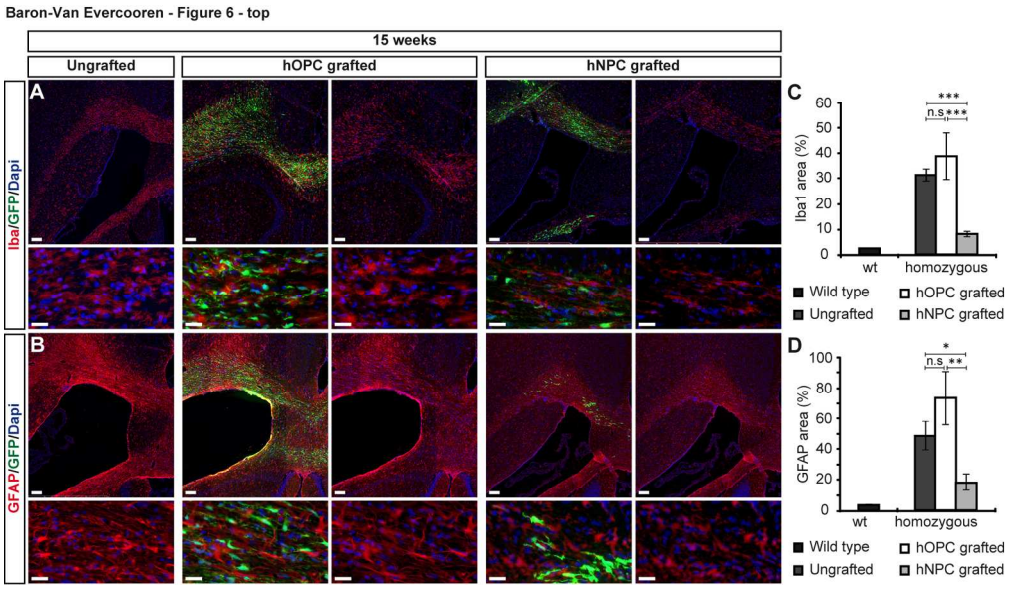

Figure 6. Human hNPCs down-regulate microglia and astrocyte loads.
(A, B) Microglial cells (A) and astrocytes (B) load at 15 weeks p.t. Microglial cells (Iba1) and astrocytes (GFAP) are stained in red while human cells (GFP) are in green, Dapi+ nuclei are in blue. Lower panels of (A) and (B) are higher magnifications of top panels. Scale bars: 100 µm higher panel, 25 µm lower panel. (C, D) Quantification of microglia (C) and astrocytes (D) densities are expressed as the percentage of Iba1 and GFAP labelled areas of the corpus callosum (ungrafted: n=3; hOPCs: n=3; hNPCs: n=9). Data are shown as mean ± SEM. *p < 0.05; **p<0.01; ***p<0.001 versus the indicated groups using Student's t test.
169x98mm (300 x 300 DPI)

For Review

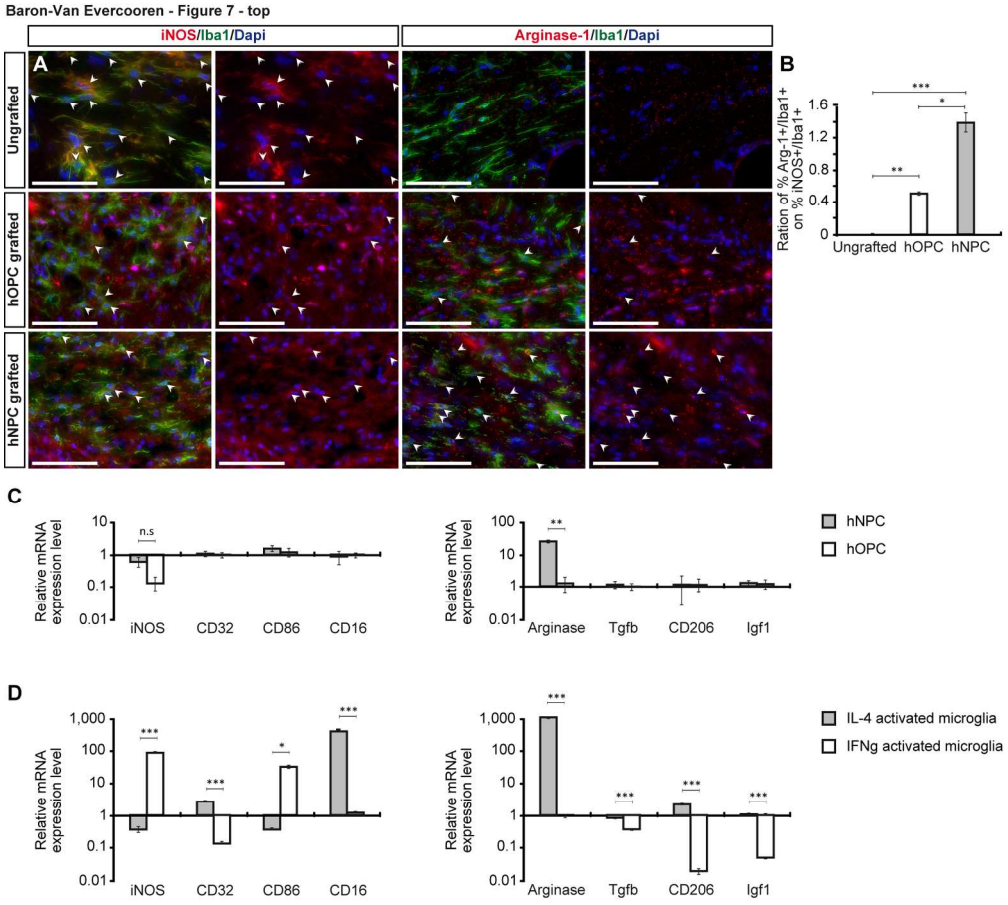

Figure 7. Human hNPCs induce a M2-like microglial phenotype.
(A) M1-like and M2-like microglia activation state are revealed by colocalization of Iba1+ cells (green) with iNOS or Arginase-1 (red) respectively. Dapi+ nuclei are in blue. The flat morphology in the ungrafted and hOPCs-grafted mice correlates with the iNOS+ M1-like activated state while the bipolar morphology of microglia in hNPCs-grafted mice correlates with the Arginase-1 M2-like state (ungrafted: n=3; hOPCs: n=3; hNPCs: n=9). Scale bars represent 50 µm. (B) Ratio of the percentage of Iba1+/Arg-1+ cells (M2-like) to the percentage of Iba1+/iNOS+ cells (M1-like). (C-D) Quantitative real-time RT-PCR highlighted modulation of classically activated M1-like and alternatively activated M2-like gene expression of (C) CD11b+ cells isolated from hNPCs- and hOPCs-grafted mice versus CD11b+ cells from ungrafted mice, and of (D) in vitro IL-4-atcivated or IFNγ-activated microglial cell versus unactivated microglia. Data are presented as values of relative gene expression after normalization with GAPDH levels. Data are shown as mean ± SEM. *p < 0.05; **p<0.01; ***p<0.001 versus the indicated groups using Student's t test.
168x151mm (300 x 300 DPI)

Baron-Van Evercooren

Supplemental Data

Figure Legends:

Supplemental Figure 1. Human NPCs and OPCs survive and migrate extensively in *Plp-tg:Rag* white matter areas.

(A) Widespread distribution of hNPCs and hOPCs throughout their host brain as viewed at different levels of transversal brain sections at 15 weeks p.t. **(B)** Quantification of hNPCs and hOPCs in the corpus callosum at 15 weeks post transplantation (n=3 per group). Error bars indicate ± SEM. **(C)** Preferential migration of human cells (hNPCs) in white matter areas: (i) corpus callosum, (ii) *fimbria*, (iii) cerebellum, (iv) striatum, (v) anterior commissure, (vi) and olfactory bulbs at 35 weeks p.t. (n=3). Scale bars: (A) 1 mm; (C) 100 µm. *p < 0.05; **p<0.01; ***p<0.001 versus the indicated groups using Student's t test.

For Peer Review

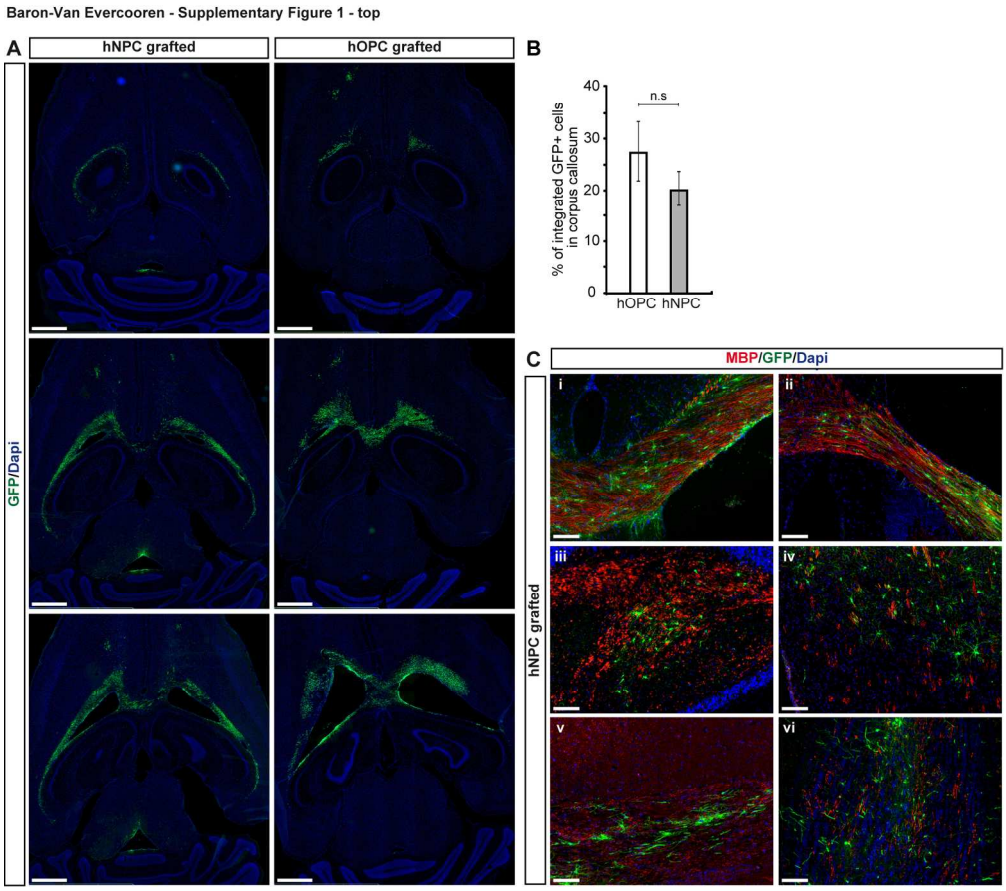

Supplementary Figure S1. Human NPCs and OPCs survive and migrate extensively in Plp-tg:Rag white matter areas.

(A) Widespread distribution of hNPCs and hOPCs throughout their host brain as viewed at different levels of transversal brain sections at 15 weeks p.t. (B) Quantification of hNPCs and hOPCs in the corpus callosum at 15 weeks post transplantation (n=3 per group). Error bars indicate ± SEM. (C) Preferential migration of human cells (hNPCs) in white matter areas: (i) corpus callosum, (ii) fimbria, (iii) cerebellum, (iv) striatum, (v) anterior commissure, (vi) and olfactory bulbs at 35 weeks p.t. (n=3). Scale bars: (A) 1 mm; (C) 100 μm. *p < 0.05; **p<0.01; ***p<0.001 versus the indicated groups using Student's t test.

169x148mm (300 x 300 DPI)